Resonant acoustic nonlinearity for defect-selective imaging and NDT

Igor Solodov

Citation: AIP Conference Proceedings **1685**, 020003 (2015); doi: 10.1063/1.4934383
View online: http://dx.doi.org/10.1063/1.4934383
View Table of Contents: http://scitation.aip.org/content/aip/proceeding/aipcp/1685?ver=pdfcov
Published by the AIP Publishing

Resonant Acoustic Nonlinearity for Defect-Selective Imaging and NDT

Igor Solodov

IKT, University of Stuttgart, 70569 Stuttgart, Germany

isolodov@ikt.uni-stuttgart.de

Abstract. The bottleneck problem of nonlinear NDT is a low efficiency of conversion from fundamental frequency to nonlinear frequency components. In this paper, it is proposed to use a combination of mechanical resonance and nonlinearity of defects to enhance the input-output conversion. The concept of the defect as a nonlinear oscillator brings about new dynamic and frequency scenarios characteristic of parametric oscillations. The modes observed in experiment include sub- and superharmonic resonances with anomalously efficient generation of the higher harmonics and subharmonics. A modified version of the superharmonic resonance (combination frequency resonance) is used to enhance the efficiency of frequency mixing mode of nonlinear NDT. All the resonant nonlinear modes are strongly localized in the defect area that provides a background for high-contrast highly-sensitive defect- and frequency-selective imaging.

INTRODUCTION

The idea of using ultrasonic nonlinear response for material characterization originated in early 1960s along with the first experimental observations of the second harmonic generation in solids [1, 2]. In flawless materials, acoustic nonlinearity is associated with lattice anharmonicity and reveals nonlinear behaviour of inter-molecular forces. It implies that the stiffness of a nonlinear material is, in principle, a function of strain that leads to a local variation of the wave velocity, waveform distortion and higher harmonic (HH) generation. However, the measurements showed that even for high ultrasonic strains $\approx 10^{-4}$ in basically all homogeneous and free from defects materials, the amplitude dependent stiffness variation is usually below 10^{-3}. As a result, noticeable nonlinear effects are developed only due to accumulation of the nonlinearity along the propagation distance (in the lack of dispersion), and, in practical terms, solely the second harmonic signal can be used for material characterization and NDT.

However, even in the first experimental studies a substantial increase in nonlinearity was noticed in materials with imperfections: a substantial enhancement of the second harmonic signal was measured in a high-purity Al single crystal in which a dislocation pattern was induced by mechanical stress applied [3]. Further investigations confirmed an important role of internal boundaries in acoustic nonlinearity enhancement for dislocations in fatigued materials [4] and matrix-precipitate interfaces in alloys [5].

A number of studies were implemented then to identify the mechanisms and manifestations of the "imperfect" nonlinearity. The experiments revealed a substantial increase of nonlinearity in weakly-bonded contacts of cracked defects due to specific contact acoustic nonlinearity (CAN) [6]. Besides the higher efficiency, CAN was shown to exhibit a qualitative departure from fundamental nonlinear effects of HH generation. The family of "NDT tags" observed for nonlinear defects included frequency down-conversion (subharmonics), hysteresis, instabilities, chaotic dynamics, etc. [7]. To interpret such unconventional effects the damaged area was assumed to manifest both nonlinear and resonance properties [8]. A direct experimental proof for the "resonant" defects has been obtained recently [9] and the concept of Local Defect Resonance (LDR) introduced.

In this paper, a combined effect of CAN and LDR on nonlinear ultrasonic response of defects is studied. Unlike the resonance of the whole specimen, LDR naturally provides an efficient energy delivery from the wave directly to the defect, so that it manifests a profound nonlinearity (efficient HH generation and frequency mixing) even at moderate ultrasonic excitation level. The LDR-induced defect nonlinearity also results in new "nonclassical" features characteristic of nonlinear and parametric resonances. It is shown that the frequency- and spatially-selective

Recent Developments in Nonlinear Acoustics
AIP Conf. Proc. 1685, 020003-1–020003-10; doi: 10.1063/1.4934383

ultrasonic activation of defects by using the concept of LDR is the way to optimize the sensitivity and efficiency of nonlinear ultrasonic imaging and NDT.

NONLINEARITY OF CRACKED DEFECTS

The strength of interface bonding is a crucial factor for development of nonlinear phenomena in fractured materials. A weakly bonded micro-scale interface of a cracked defect driven by an intense ultrasonic wave displays a specific nonlinear dynamics of an intermittent contact associated with either symmetrical or asymmetrical stiffness variation when driven by the in-plane or out-of-plane tractions, respectively.

Compression-tension of a contact between defect elements (clapping) apparently, results in asymmetrical modulation of the local stiffness: it is higher for compression and lower for contact extension. Such "bimodular" behaviour can be approximated by a piece-wise stress-strain relation [10]:

$$\sigma = [C_0 - H(\varepsilon - \varepsilon^0)\Delta C]\varepsilon, \tag{1}$$

where $H(\varepsilon)$ is the Heaviside function; ΔC is the modulation depth of the compressed (ε^0 is the pre-strain) contact stiffness (C_0) that, generally, can be much higher than that in the classical (flawless) case. The Taylor series expansion of the nonlinear term in (1) brings about multiple both odd and even HH generated locally in the defect area as soon as $\varepsilon > \varepsilon^0$. Due to a pulse-type stiffness variation, the HH amplitudes are modulated by the *sinc* envelope function. The clapping model results in an unusual nonlinear waveform distortion: the interface acts as a mechanical diode with a rectified output.

For an in-plane drive, the contact interface is mechanically coupled by the friction force caused by the interaction between asperities. A small amplitude in-plane motion of the interface is constrained by the interaction between neighbouring group of asperities that prevents the micro-contact surfaces from sliding (micro-slip mode). The model leads to a step-wise increase in tangential contact stiffness as the neighbouring asperities interact:

$$\sigma = \left\{ C_0 - [H(\varepsilon + \varepsilon^0) - H(\varepsilon - \varepsilon^0)]\Delta C \right\} \varepsilon \tag{2}$$

This interaction is independent of the direction of in-plane motion (symmetrical nonlinearity) and provides only odd harmonic generation. Similar to the clapping mechanism, their amplitudes are *sinc*-modulated due to pulse-type stiffness modulation.

In realistic defects, normally both CAN mechanisms are triggered and result in efficient multiple HH nonlinear spectra [11]. Provided the defect exhibits LDR (see below) the nonlinear vibrations are being "locked" inside the defect area. This makes CAN inherently defect-selective and set up the background for defect-selective nonlinear imaging of fractured flaws. Fortunately, this group of flaws includes the most typical defects in composite materials: micro- and macro-cracks, delaminations, disbonds, impact damages, etc. which will be discussed within the scope of this paper.

LDR: CONCEPT AND SIMULATIONS

The concept of LDR is based on the fact that inclusion of a defect leads to a local decrease in stiffness of a certain mass of the material in this area, which should manifest in a particular characteristic frequency of the defect. The LDR frequency can be introduced as a natural frequency of the defect with an effective rigidity K_{eff} and mass M_{eff}: $f_0 = \frac{1}{2\pi}\sqrt{K_{eff}/M_{eff}}$. To derive the expressions for K_{eff} and M_{eff} one should evaluate the potential and kinetic vibration energy of the defect [12]. To clarify the physical nature of LDR this approach is applied to model defects such as flat-bottomed holes (FBH). For a circular FBH (radius R, thickness h), the expressions obtained are:

$$K_{eff} = 192\pi D/R^2;\ M_{eff} = 1.8m, \tag{3}$$

while for a square FBH (side a and thickness h):

$$K_{eff} = 32\pi^4 D/a^2;\ M_{eff} = 2.25m, \tag{4}$$

where $D = Eh^3/12(1-\nu^2)$ is the bending stiffness, E is Young`s modulus, $\nu$ is Poisson`s ratio, and m are the masses of the plates with density ρ in the bottom of the defect.

Equations (3-4) are then combined to yield the LDR frequencies for the defects in question:

$$f_0 = \frac{10h}{3\pi R^2}\sqrt{\frac{E}{5\rho(1-\nu^2)}}. \tag{5}$$

$$f_0 = \frac{4\pi h}{3a^2}\sqrt{\frac{E}{6\rho(1-\nu^2)}}. \tag{6}$$

The expressions for f_0 obtained above are applicable to evaluation of the fundamental resonance frequencies of the defects, like FBH as well as laminar defects in rolled sheet metals and delaminations in composites. For example, the application of (6) to a square FBH in PMMA ($h = 1.2$ mm; $a = 2$ cm) yields: $f_0 = (7.2 \div 9.4)$ kHz for Young`s modulus variation in the range $(1.8 \div 3.1)$ GPa given in the literature.

The problem in practical use of the analytical approach is concerned with the boundary conditions for the defect edges, which were assumed to be clamped in deriving (5) & (6). This is apparently justifiable for "deep" FBH in plates, however, in a general case the analytical formulation presented above becomes problematic. Instead, the finite element simulation was used to visualize the LDR vibration patterns and to evaluate the LDR frequencies.

The software COMSOL MULTIPHYSICS (physics package "structural dynamics," "eigenfrequency analysis") was found to be suitable for analyzing the vibration characteristics of structures with defects and to determine the LDR frequencies. By using eigenfrequency analysis of the model, each possible resonance of vibrations in the plate can be found and the vibration patterns plotted. Figure 1 illustrates the vibration pattern at frequency 8255 Hz, which is readily identified as a fundamental LDR of a square FBH ($h = 1.2$ mm; $a = 2$ cm). Note, that the value of f_0 obtained is well within the frequency range covered by Eq. (6). A similar "bell-like" vibration pattern reveals a fundamental LDR in a circular FBH at frequency 10.4 kHz (Fig. 2 (a)), followed by the higher-order LDR at the higher driving frequency of 23.25 kHz (Fig. 2 (b)).

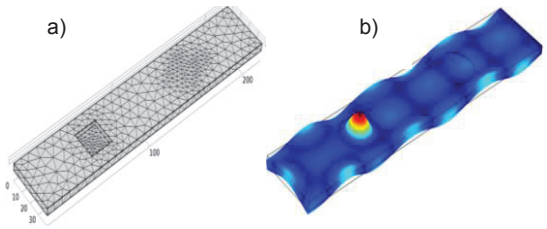

FIGURE 1. FEM mesh (a) and fundamental LDR vibration pattern at $f_0 = 8255$ Hz (b) for 2x2 cm^2 square FBH in a PMMA plate.

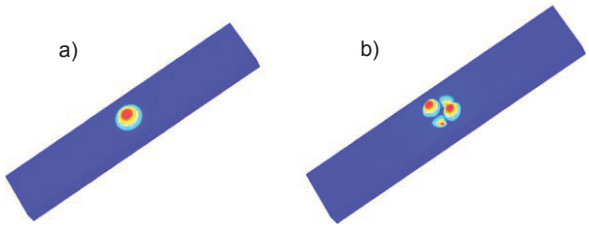

FIGURE 2. A fundamental LDR (10.4 kHz) (a) and higher-order LDR (23.25 kHz) (b) for a FBH (radius 1 cm, depth 2 mm) in a PMMA plate (thickness 3 mm).

LDR EXPERIMENTAL EVIDENCE

A direct way to experimentally reveal LDR is to measure an individual contribution of each point of the specimen in its overall frequency response. For this purpose, an ultrasonic excitation by a wide-band piezoelectric transducer is combined with a laser vibrometer (PSV 300 Polytec) scan of the specimen surface. It enables to probe and indicate all possible resonances in every point of the specimen. The origin of each maximum is then verified by imaging the vibration patterns in the specimen at the corresponding frequency. A strong enhancement of the vibration amplitude observed locally in the defect area is identified as a fundamental defect resonance.

Figure 3 illustrates LDR frequency responses and the vibration patterns measured for a simulated (circular FBH in PMMA plate) and a realistic defect (impact damage in carbon fiber reinforced composite (CFRP)). LDR feature a strong enhancement of the vibration amplitude confined strictly inside the defect areas with high Q-factors (in Fig. 3, $Q \approx 75$ for FBH and $Q \approx 85$ for the impact damage). The value of Q factor determines the resonance "amplification" of the vibration amplitude. Similar measurements showed that the quality factors in the range of 10-100 are typical for realistic defects in composites so that the LDR induced "amplification" of local vibrations as high as ~ 20-40 dB was usually observed.

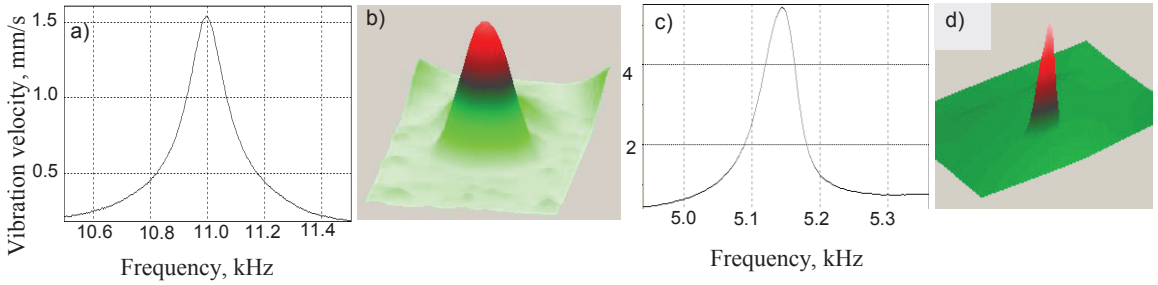

FIGURE 3. LDR frequency responses and vibration patterns for a circular flat-bottomed hole (radius a=1 cm; depth h=0.8 mm) in PMMA plate (200x30x3mm^3) (a, b) and impact damage in CFRP plate (c, d).

LDR NONLINEARITY

Since LDR is as an efficient resonant "amplifier" of the local vibrations, one would expect it to contribute appreciably to defect nonlinearity. An extremely high resonant nonlinearity is demonstrated in Fig. 4 for a delamination in GFRP plate: Multiple HH generation is observed even at a moderate input voltage. A crucial role of the driving frequency match to LDR for increase of nonlinearity is illustrated in Fig. 5 for a crack in a unidirectional (UD-) CFRP rod. As the driving frequency matches the LDR frequency (19.5 kHz), a strong enhancement of the HH amplitudes generated locally in the defect area is observed.

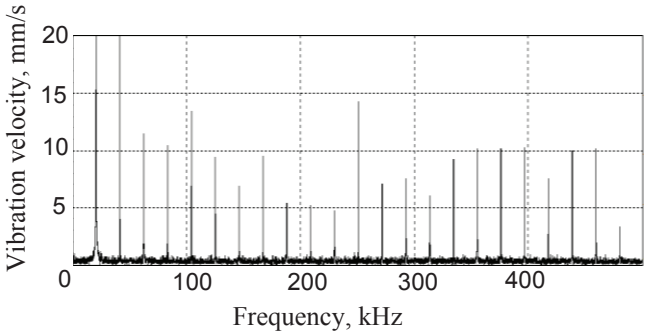

FIGURE 4. HH spectrum for delamination in GFRP specimen driven at LDR frequency 20900 Hz. Input voltage is 7 V.

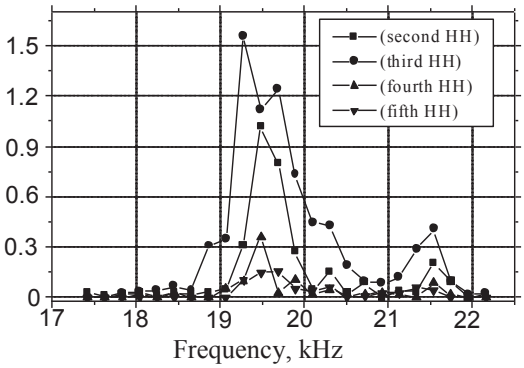

FIGURE 5. HH LDR frequency response of a crack in CFRP rod (LDR frequency 19.5 kHz).

The LDR-induced enhancement of nonlinearity can also be applied for efficient frequency mixing. In the experiment, two contra-flowing flexural waves insonified an impact damage (LDR frequency band 100-120 kHz shown in Fig. 10) in a CFRP plate. The frequency of one of the waves (f_1 = 111500 kHz) was chosen inside the LDR band while the frequency of the second wave (f_2) was swept within 80-130 kHz bandwidth. The spectrum of LDR vibrations (Fig. 6) is highly sensitive to the frequency match between f_2 and LDR (Fig. 7) so that multiple mixed frequency components are generated only as soon as both frequencies are inside the LDR band. The spectrum is well described by $mf_1 \pm nf_2$ combination produced by the ($m+n$)-order of nonlinear interaction. The side-lobe

pattern in Fig. 6 reveals that the nonlinear interactions up to the 10th –order are developed by combining CAN and LDR.

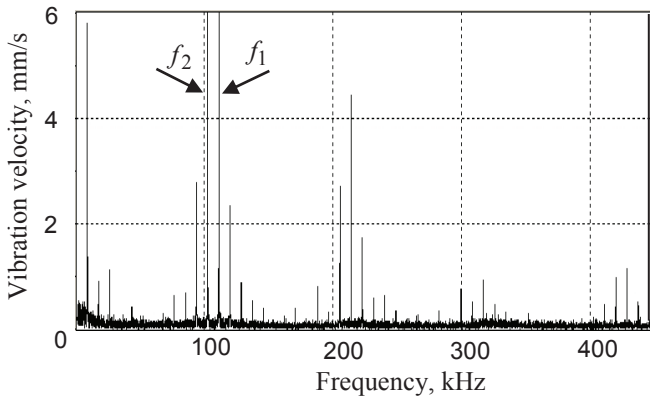

FIGURE 6. Mixing frequency spectrum in an impact damage in a CFRP plate: $f_1 = 111500$ Hz; $f_2 = 102800$ Hz.

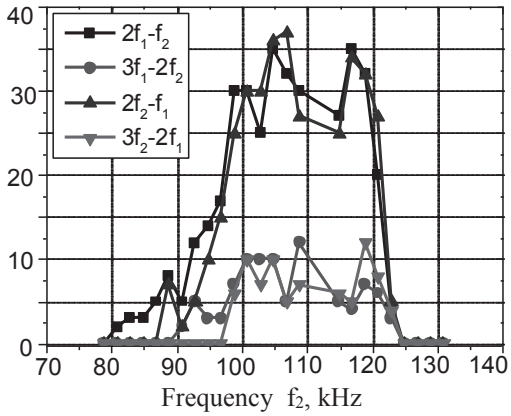

FIGURE 7. Variation of mixed frequency amplitudes as functions of f_2 frequency sweep around LDR.

The results presented in Figs. 4-6 prove that at moderate input signals the LDR enhances appreciably the nonlinearity of defects via local "amplification" of vibrations. It raises substantially the efficiency of "conventional" nonlinear effects, like HH generation and frequency mixing. However, this is not the only dynamic scenario of nonlinear phenomena for resonant defects. At higher level of excitation, a combined effect of LDR and nonlinearity can result in qualitatively new features characteristic of nonlinear and parametric resonances.

Superharmonic Resonances

To analyse the effect of nonlinearity on resonant vibrations of a defect the second and third-order nonlinear terms are introduced in the equation of forced vibrations of an oscillator with natural frequency ω_0 [13]:

$$\ddot{x} + 2\lambda\dot{x} + \omega_0^2 x + \alpha x^2 + \beta x^3 = F_0 \cos \nu t \quad , \tag{7}$$

where λ is the dissipation factor, α and β are the corresponding factors in the series expansion of the stress-strain relation (parameters of nonlinearity).

For the superharmonic resonance, the input frequency is taken as $\approx \omega_0 / n$ and converted into ω_0 drive via the nth-order nonlinearity of the oscillator. The example given below corresponds to $n = 2$ and uses the perturbation approach for finding solutions to equation (7).

For the driving frequency $\nu = (\omega_0 / 2) + \varepsilon$ and small λ , the solution of the first approximation is a non-resonant linear driven vibration:

$$x_1 = \frac{4F_0}{3\omega_0^2} \cos[(\omega_0 / 2) + \varepsilon)t] \tag{8}$$

The resonance driving force will be developed directly via quadratic nonlinearity so that after inserting (8) in (7) and keeping only resonant terms in the right hand side, one obtains:

$$\ddot{x}_2 + 2\lambda\dot{x}_2 + \omega_0^2 x_2 + \alpha x_2^2 + \beta x_2^3 = -\alpha x_1^2 \cos(\omega_0 + 2\varepsilon) \tag{9}$$

A solution to (9) could be readily found if one neglects the nonlinear terms of the second-order solution in the left-hand side:

$$x_2^{2\omega} = \frac{4\alpha F_0^2}{9\omega_0^5 \sqrt{4\varepsilon^2 + \lambda^2}} \cos[(\omega_0 + 2\varepsilon)t] \quad . \tag{10}$$

A similar procedure for the input $\nu = (\omega_0 / 3) + \varepsilon$ leads to the solution for the resonant third HH:

$$x_2^{3\omega} = \frac{\beta (x_1^0)^3}{8\omega_0 \sqrt{9\varepsilon^2 + \lambda^2}} \cos[(\omega_0 + 3\varepsilon)t] \quad , \tag{11}$$

where $x_1^0 = 9F_0 / 8\omega_0^2$.

Equations (10) & (11) confirm the resonant generation of the second and third higher harmonics. The maximal amplitudes of the superharmonic resonances reduce with n ($\sim F_0^n$) but also depend on the values of the high-order nonlinearity. Since a step-wise stiffness modulation by means of CAN enhances its higher-order parameters, one can expect a strong development of the HH resonances in resonant defects.

A direct proof of superharmonic resonances in defects is demonstrated for the third-order resonance in impact damaged CFRP specimen with LDR around 5140 Hz in Figs. 8 & 9. One-third of the LDR frequency (1714 Hz) was therefore selected for the excitation while the input voltage was increased up to 80 V. The spectrum (Fig. 8) measured in the defect area illustrate the dominance of the third harmonic vibration (25 dB higher than the fundamental, Fig. 8) also proved by quite "clean" third harmonic vibration pattern (period ~0.19 ms in Fig. 9). Because of the high-Q fundamental LDR (Fig. 3, c), the superharmonic resonance required quite precise one-third of LDR frequency placing within 100 Hz.

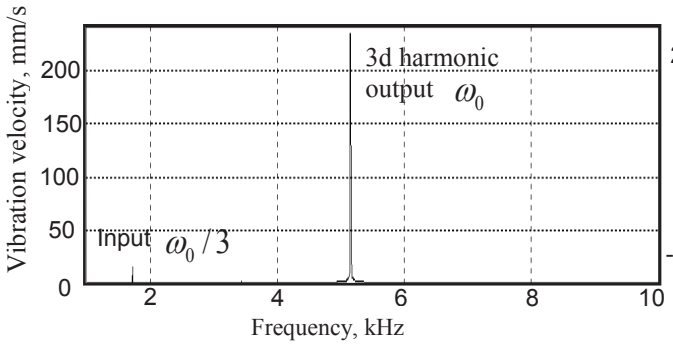

FIGURE 8. Spectrum of the third-order superharmonic LDR in impact damaged CFRP plate.

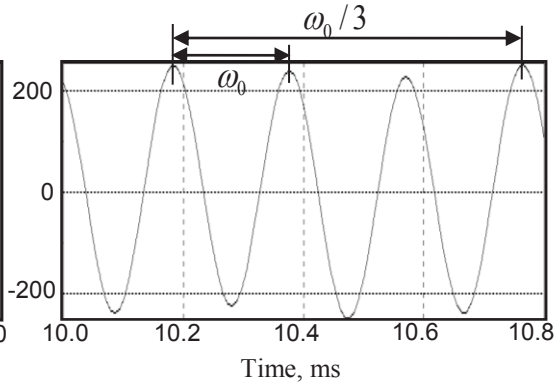

FIGURE 9. Vibration pattern of the third-order superharmonic LDR in impact damaged CFRP plate.

Combination Frequency Resonance

A high quality factor of LDR can also be used as a resonant "amplifier" in the frequency mixing nonlinear NDT. The method is based on the nonlinear interaction of ultrasonic waves of different frequencies (ν_1, ν_2) that results in a combination frequency output: $\nu_\pm = \nu_1 \pm \nu_2$. For a bi-frequency excitation of a nonlinear defect, the equation of motion is:

$$\ddot{x} + 2\lambda\dot{x} + \omega_0^2 x + \alpha x^2 + \beta x^3 = F_1 \cos\nu_1 t + F_2 \cos\nu_2 t \quad , \tag{12}$$

with the first-order (linear) solution:

$$x_1 = x_1^{\nu_1} \cos\nu_1 t + x_1^{\nu_2} \cos\nu_2 t \quad , \tag{13}$$

where $x_{1,2}^{\nu_{1,2}} = \dfrac{F_{1,2}}{\nu_{1,2}^2[(\omega_0^2 / \nu_{1,2}^2) - 1)}$.

The second-order term in (12) yields the driving force:

$$-\alpha x_1^2 = -\alpha x_1^{\nu_1} x_2^{\nu_2} [\cos(\nu_1 + \nu_2) + \cos(\nu_1 - \nu_2)] \quad , \tag{14}$$

which for the condition of frequency match $\nu_1 \pm \nu_2 = \omega_0 + \varepsilon$ brings the resonant solution:

$$x_2^{\pm} = -\frac{\alpha x_1^{\nu_1} x_1^{\nu_2}}{2\omega_0\sqrt{\varepsilon^2+\lambda^2}}\cos[(\omega_0+\varepsilon)t]. \qquad (15)$$

An application of LDR as a resonant "frequency mixing amplifier" for realistic defects is illustrated then in Figs. 10 & 11 for an impact-induced damage (area ~5x5mm^2) in a CFRP plate (280x40x1mm^3). A linear LDR frequency response of the impact demonstrates a well-defined double-maxima peak around 110 kHz (Fig. 10). The frequency of one of the interacting flexural waves was fixed at $f_1 = 77.5$ kHz while the other was swept from $f_2 = 28.5$ to 37.5 kHz to provide the sum frequency variation around the LDR frequency.

The amplitude frequency response measured with laser vibrometer at the sum frequencies shown in Fig. 11 demonstrates unambiguously the effect of the resonance: more than 20 dB increase in the output is observed when the sum frequency matches the frequency of LDR. Similar to the LDR mixing considered above, the resonant nonlinear interaction was not limited to the first-order mixing: the higher-order mixed components $mf_1 \pm nf_2$ for $m,\ n$ up to 5 were also generated in the damaged area.

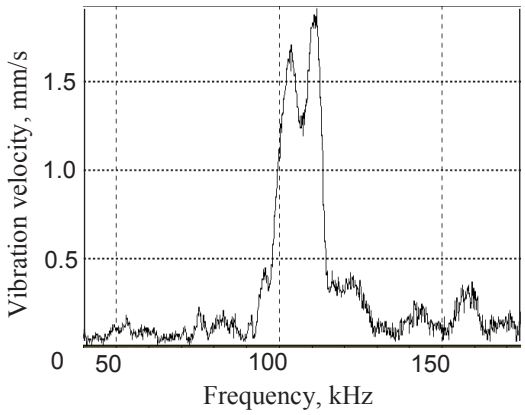

FIGURE 10. LDR frequency response for an impact induced damage in a CFRP plate.

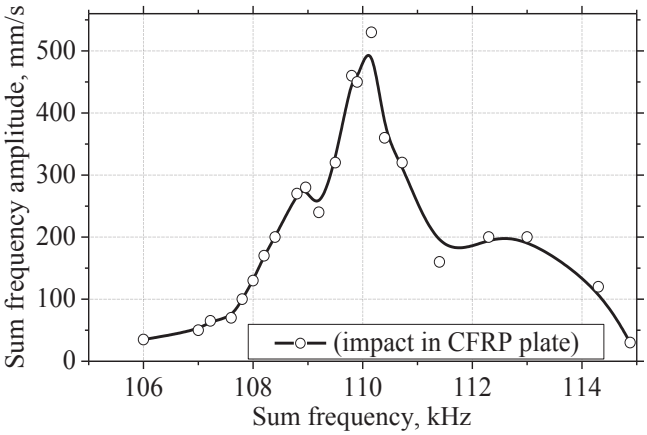

FIGURE 11. LDR induced amplification at the sum frequency vibration for impact damage in a CFRP plate.

Subharmonic and Parametric Resonances

Manifestation of parametric effects is due to the amplitude-dependent shift (modulation) of LDR frequency induced by the driving signal. The frequency shift induced by the driving signal causes a periodic modulation of the oscillator natural frequency that activates manifestation of the parametric resonance. The parametric approach (well developed and applied in many fields of physics) enables further to reveal other features of the nonlinear resonance phenomena.

The nonlinear source of parametric resonance effects can be disclosed by applying the perturbation method to equation (7). For the driving frequency close to the resonance $\nu = \omega_0 + \varepsilon$, the solution of the first approximation is a linear vibration:

$$x_1 = \frac{F_0}{2\omega_0\sqrt{\varepsilon^2+\lambda^2}}\cos\nu t \quad . \qquad (16)$$

In the next approximation, the quadratic nonlinearity in (7) apparently produces the third-order interaction term $\sim 2\alpha x_1 x_2$. By using (16) and taking into account this term only, one obtains:

$$\ddot{x}_2 + 2\lambda\dot{x}_2 + \omega_0^2[1+\frac{\alpha F_0}{\omega_0^3\sqrt{\varepsilon^2+\lambda^2}}\cos\nu t]x_2 = 0 \quad . \qquad (17)$$

Equation (17) is a Mathieu`s-type equation whose general form is:

$$\ddot{x} + \omega_0^2(1 + h\cos\gamma t)x = 0 \tag{18}$$

and which is known to reveal parametric resonance and instability phenomena [14, 15].

The form (17) corresponds to the second-order parametric resonance at $\nu \approx \omega_0$. In this case, the frequencies of the solutions to (18) include the HH of the input signal: $\omega = n\nu$ (n=1, 2, 3,..) [15]. Beyond the input threshold, their amplitudes grow in time exponentially (instability).

In a similar way, for $\nu \approx 2\omega_0$ drive, the second approximation in (7) yields [13]:

$$\ddot{x}_2 + 2\lambda\dot{x}_2 + \omega_0^2[1 - \frac{2\alpha F_0}{3\omega_0^4}\cos[(2\omega_0 + \varepsilon)t]x_2 = 0\,, \tag{19}$$

which is a condition for a subharmonic (fundamental parametric) resonance. In this case, the solutions to (19) comprise unstable ultra-subharmonic outputs: $\omega = m\nu/2$ (m=1, 2, 3,..) [15].

Unlike conventional (linear) resonance, in a certain range of detuning ε the parametric resonances provide an exponential growth of the vibration amplitudes in time even in the presence of damping. The instability develops as soon as the frequency modulation index h (input energy) exceeds a certain threshold determined by the energy dissipated in the system. The critical values of h are the functions of ε (and vice versa): the higher modulation is generally required for larger frequency mismatch thus producing divergent boundaries of the V-shaped $h(\varepsilon)$ curves for parametric resonances [15]. Thus, for high modulation amplitudes, the parametric resonances can be observed in broad frequency bands.

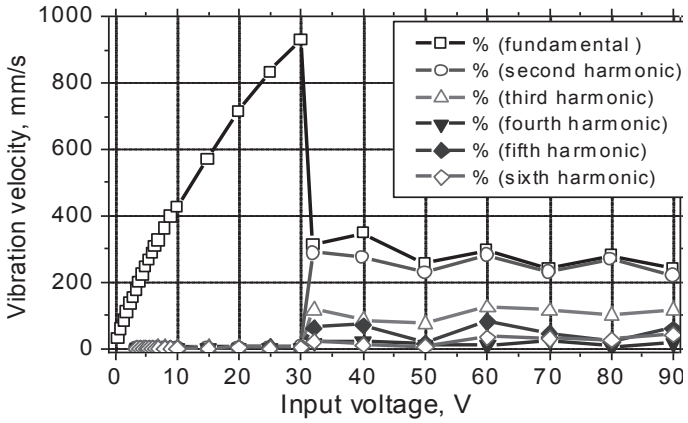

FIGURE 12. Bifurcation nonlinear dynamics of resonant HH generation for an impact damage in a CFRP plate.

The experimental proof for unstable parametric dynamics of the HH (the second-order parametric resonance) is given in Fig. 12 for impact damage (LDR at 5140 Hz, Fig. 3, c) in CFRP sample. The nonlinear regime starts above a step-like instability threshold at ~30V input (Fig. 12) and results in a strong nonlinear distortion of vibrations with highly nonlinear spectrum of HH. This behavior is in accord with general theoretical analysis for parametric resonances: Beyond the threshold input at fundamental LDR frequency the parametric resonances are activated and provide an instable growth of the HH. The fundamental vibration is depleted due to the energy outflow and heavily distorted via frequency conversion to HH.

The excitation frequency was then changed to the second harmonic (10280 Hz) of the fundamental LDR to observe a subharmonic resonance. The threshold for the resonance was found to be $\approx$45 V as illustrated in Figs. 13, a), b). Beyond the threshold, the subharmonic component increases dramatically and prevails in the vibration (velocity) spectrum: $V_{\omega/2}/V_{\omega} \approx 30$ dB at 10280 Hz input (Fig. 13, b)). This complies with pure sinusoidal subharmonic vibration pattern in the impact area beyond the threshold (Fig. 13, a)). The input frequency range for both subharmonic and superharmonic resonances was measured to be within ~100-200 Hz that corresponds to a high Q factor of the LDR for this defect.

LDR NONLINEAR DEFECT-SELECTIVE IMAGING

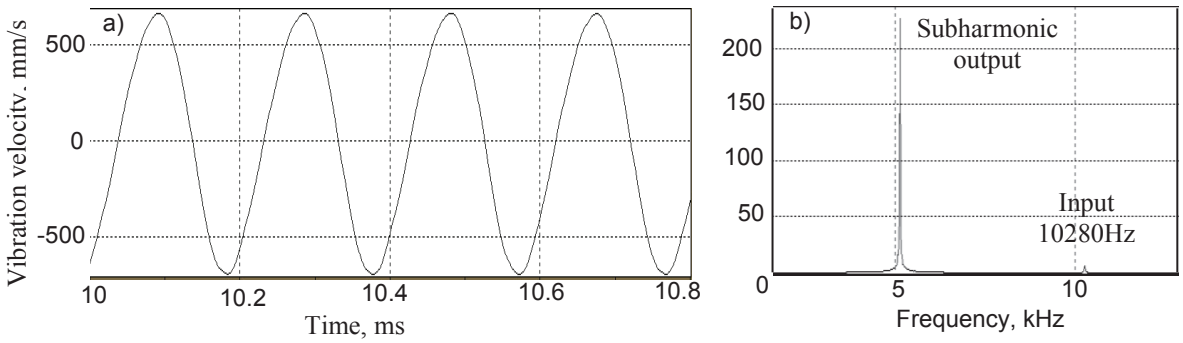

FIGURE 13. Subharmonic LDR for impact damage in CFRP: vibration patterns (a) and spectrum (b) beyond threshold input voltage 45 V.

According to the above, under LDR condition, new nonlinear frequency components are generated efficiently so that the input power can be reduced substantially. In our experiments and applications, the input electric power is usually well below 1W; general purpose piezo-ceramic transducers (Conrad Elektronik GmbH) are used for ultrasonic excitation without any particular filtering of the input signals. Besides, due to LDR the nonlinear vibrations are being confined inside the defect area. This makes LDR nonlinearity inherently defect-selective and provides the background for defect-selective nonlinear imaging of fractured flaws.

The benefit of the higher harmonic LDR imaging is illustrated in Fig. 14. A substantial improvement of the image quality (10x20 mm^2 delamination in a GFRP plate) is clearly seen by comparing the fundamental (signal-to-noise ratio ~12 dB) and the second harmonic (signal-to-noise-ratio ~24 dB) images.

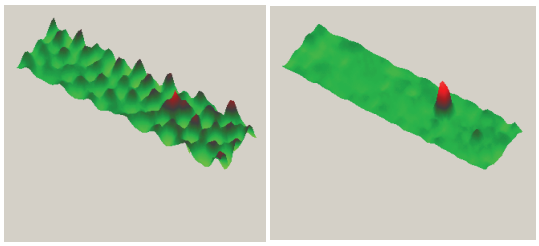

FIGURE 14. Linear (36.77 kHz, a) and second harmonic (73.53 kHz, b) LDR imaging of a delamination in GFRP specimen.

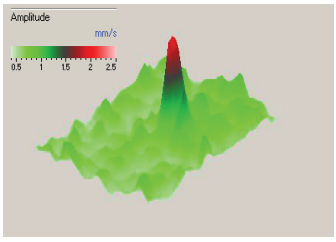

FIGURE 15. Sum-frequency image of impact damage (~5x5mm^2) in a CFRP plate.

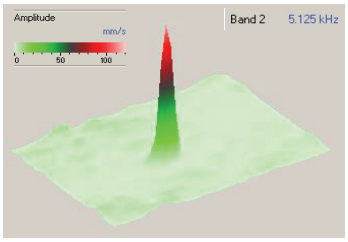

FIGURE 16. Subharmonic LDR imaging of impact damage: Input 10250 Hz; output 5125 Hz.

Other examples of the resonance nonlinear imaging are given in Figs. 15, 16. The LDR contribution to the sum-frequency signal makes it localized in the damage area and enables to be used for mixing frequency imaging with reasonable signal-to-noise level (~15 dB, Fig. 15). This image of the impact in a CFRP plate was obtained by mixing flexural waves of frequencies 77 kHz and 30 kHz via combination frequency resonance (LDR frequency of the defect 107 kHz). The benefit of subharmonic LDR is illustrated in Fig. 16 for the impact damage in CFRP specimen.

CONCLUSIONS

A low efficiency of conversion from fundamental frequency to nonlinear frequency components is a long-term bottleneck problem of nonlinear ultrasonic applications in NDT. In this paper, it is proposed to use a combination of nonlinearity with Local Defect Resonance (LDR) to enhance substantially the efficiency of nonlinear frequency conversion by the defects. Since LDR is as a resonant "amplifier" of the local vibrations, it manifests a profound nonlinearity and efficient generation of the HH and combination frequency components even at moderate ultrasonic excitation level. These "classical" nonlinear effects, however, are not the only dynamic scenario of nonlinear

phenomena for resonant defects. A combined effect of LDR and nonlinearity results in qualitatively new "nonclassical" features characteristic of nonlinear and parametric resonances.

The experiments confirm unconventional nonlinear dynamics of realistic defects subject to LDR and demonstrate that the nonlinear resonance and parametric dynamics should be seen not as exceptional or anomalous but rather conventional and peculiar to majority of defects in the resonance conditions. The threshold transition to a strongly nonlinear resonance mode is accompanied by instability of vibrations. Beyond the threshold, the instability ceases and the vibration returns to stability via a strong rise of nonlinear frequency up-conversion.

According to the experiments, under resonance conditions the nonlinear components, like HH, mixed frequencies, and subharmonics may dominate in the vibration spectrum of defects. This suggests nonlinear LDR application as an extremely efficient mode in nonlinear NDT. Besides, both super- and subharmonic LDR are strongly localised in the defect area that brings about an opportunity for high-contrast defect-selective imaging. The resonant nonlinear modes require much lower acoustic power to activate the defects that makes it possible to avoid high-power instrumentation and use conventional ultrasonic NDT equipment instead.

ACKNOWLEDGEMENTS

The author acknowledges support of this study in the framework of ALAMSA project funded from the European Union's Seventh Framework Programme for research, technological development and demonstration under grant agreement no. 314768.

REFERENCES

1. A. A. Gedroits, V. A. Krasilnikov, and L. K. Zarembo, Acustica **3**, 2, 108 (1963).
2. M. A. Breazeale and D. O. Thompson, Appl. Phys. Letters, **3**, 5, 77-78 (1963).
3. A. Gedroitz and V. A. Krasilnikov, Sov. Phys. JETP, **16**, 1122-1131 (1963).
4. W. T. Yost and J. H. Cantrell, Rev. Progress QNDE, **9**, 1669–1676 (1990).
5. J. Cantrell and W. Yost, J. Appl. Phys., **81**, 2957-2962 (1997).
6. I. Solodov, Ultrasonics, **36**, 383-390 (1998).
7. I. Solodov and B. Korshak, Phys. Rev. Letters, **88**, 014303 (2002).
8. I. Solodov, J. Wackerl, K. Pfleiderer and G. Busse, Appl. Phys. Letters, **84**, 5386-5388 (2004).
9. I. Solodov, J. Bai, S. Bekgulyan, and G. Busse, Appl. Phys. Letters, **99**, 211911 (2011).
10. I. Solodov, N. Krohn, and G. Busse, Ultrasonics, **40,** 621-625 (2002).
11. I. Solodov, K. Pfleiderer, and G. Busse, "Nonlinear Acoustic NDE: Inherent potential of complete nonclassical spectra" in *Universality of Nonclassical Nonlinearity with Application to NDE and Ultrasonics*, edited by P. Delsanto (Springer Verlag, New York, USA, 2006), pp. 465-484.
12. S. P. Timoshenko, *Vibration Problems in Engineering* (D. Van Nostrand Company, 4th Ed., 1956).
13. L. D. Landau and E. M. Lifshitz, *Mechanics* (Pergamon Press, 1960).
14. N. W. McLachlan, *Theory and Applications of Mathieu functions* (University Press, Oxford, 1951).
15. E. K. Kneubuehl, *Oscillations and Waves* (Springer, Berlin, 1997).